

# NUMERICAL INVESTIGATION OF LIQUID JET INJECTION INTO A SUPERSONIC CROSSFLOW

Haixu Liu, Yincheng Guo, Wenyi Lin

Department of Engineering Mechanics, Tsinghua University, Beijing 100084, China

**Keywords:** *two-fluid model, liquid jet, supersonic crossflow, penetration height*

## Abstract

*Numerical study of liquid jet injection into a supersonic crossflow was carried out using two-fluid model. A  $k-\varepsilon-k_p$  turbulence model is employed for simulating two-phase compressible turbulent flow. As the authors know, it is the first time to extend the two-phase turbulence model into the compressible multiphase flow, despite its commonly applications in the incompressible regimes. Separation of the boundary layer in front of the liquid jet was predicted with the induced separation shock wave. A bow shock wave caused by the injection was formed and interacts with the separation shock wave. The predicted penetration height is in good agreement with the experimental data. In addition, the turbulent kinetic energy of both the gas and droplet phase were presented for comparisons, and the effects of the jet-to-air momentum flux ratio and droplet diameters on the penetration height were also examined in this work.*

## 1 Introduction

The description of liquid jet injection into a supersonic primary flow has become an important research area as the development of high-speed flight vehicles. Such a process is encountered in thrust vector control, external burning on projectiles, and particularly in the design of scramjet engines. For high-performance of propulsion, the combustion efficiency depends strongly on the breakup, atomization and evaporation of liquid fuel jet [1-4]. The penetration of fuel jet injection into the combustor has a great effect on the diffusive

mixing of fuel and free stream air, which is needed for the preconditions of chemical reaction. However, the interaction between the two fluid streams is accompanied by boundary-layer separation and recirculation on the wall near the jet injection. The complexity of the mechanism makes it difficult for detailed analysis from a theoretical point, especially for the compressible two-phase flow.

The liquid injection into a crossflow of air has been studied in numerous investigations previously [5-7]. Based on these works, a jet plume model has been devised, and the schematic of the liquid jet into high-speed crossflow is shown in Fig. 1. In front of the injected liquid jet, a bow shock is formed due to the resistance of the jet, while the adverse pressure gradient causes the boundary layer to detach, resulting in the separation shock. The separation and bow shocks interact and modify the bow shock angle and jet flow direction, which is called “whipping phenomena”. The appearance of the separation shock is of importance in cases involving fuel jet mixing with the air and the combustion considering its flame-holding capability. As the jet penetrates into the crossflow, the jet is deflected and subjected to wavelike disturbances, yielding the primary breakup in the form of clump detachment. After that, the secondary breakup gives rise to smaller droplets under action of the aerodynamic forces of the crossflow.

There are several parameters, such as droplet size, droplet velocity, and liquid volume flux distribution to be considered in the investigations, and one of the global parameters that indicates the mixing condition of the injected liquid with the freestream air is the penetration height of the liquid jet, which is also

needed for the preconditions of chemical reaction.

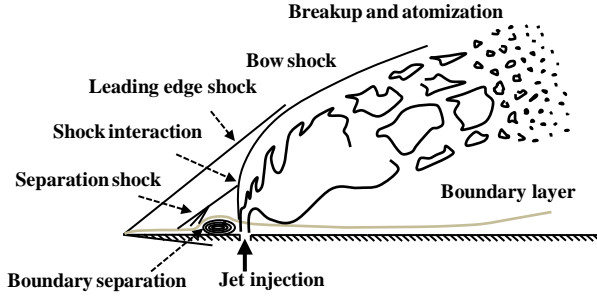


**Fig. 1 Schematic of liquid jet injection into supersonic flow.**

Many experimental studies have been devoted to the liquid jet's penetration height into supersonic flow, considering the importance related to the mixing performance and combustion efficiency. Several empirical correlations have been formulated experimentally to predict the penetration height of the liquid jet into subsonic or supersonic crossflows [8-12]. However, limited numerical investigations are seen in the literatures, which is an efficient way for the study of compressible two-phase flow. There are mainly two approaches to investigate the two-phase flow problem. One is the Euler-Lagrange method, which focuses on a single particle trajectory, and obtains the flow field after the computation of interaction between the fluid and all of the particles, resulting in a lot cost of simulation time. The other one is the Euler-Euler method, which views all the particles as a continuum fluid phase, and averages out motion on the scale of individual particles, and it enormously reduces the simulation cost.

The Euler-Euler method has been widely used in simulations of incompressible two-phase flow [13, 14]. However, for compressible two-phase flow, most of the researches ignored the viscosity and fluctuations of the particle phase, but the interaction between the two phases is so strong that it is necessary to adapt appropriate model to take the turbulence of the particle phase into account.

In this work, the Navier-Stokes equations in a conservation form for compressible gas flow were solved. The mass, momentum and energy equations of the droplet phase in the Eulerian-Eulerian framework were conveniently

expressed corresponding to the gas phase. A  $k-\varepsilon-k_p$  turbulence model was applied in the current turbulence simulation of liquid jet injection into a supersonic crossflow.

## 2 Mathematical Modeling

### 2.1 Governing equations for gas phase

The compressible conservative form governing equations for the gas phase are expressed as follows:

Gas phase continuity equation

$$\frac{\partial \rho}{\partial t} + \frac{\partial}{\partial x_j} (\rho v_j) = 0, \quad (1)$$

Gas phase momentum equation

$$\begin{aligned} & \frac{\partial \rho v_i}{\partial t} + \frac{\partial}{\partial x_j} (\rho v_j v_i) \\ & = -\frac{\partial p}{\partial x_i} + \frac{\partial \tau_{ij}}{\partial x_j} + \frac{\rho_p}{\tau_{rp}} (v_{pi} - v_i) \end{aligned}, \quad (2)$$

Gas phase energy equation

$$\begin{aligned} & \frac{\partial}{\partial t} (\rho E) + \frac{\partial}{\partial x_j} \left[ \rho v_j \left( E + \frac{p}{\rho} \right) \right] \\ & = \frac{\partial v_i \tau_{ij}}{\partial x_j} - \frac{\partial}{\partial x_j} \left( \lambda \frac{\partial T}{\partial x_j} \right) - n_p Q_p \end{aligned}, \quad (3)$$

where  $\rho_p$  and  $n_p$  are the density of droplet phase and number of the droplets per unit volume, respectively, and the subscript "p" represents the droplet phase. The stress  $\tau_{ij}$  is given by

$$\tau_{ij} = \mu_e \left( \frac{\partial u_i}{\partial u_j} + \frac{\partial u_j}{\partial u_i} \right) - \delta_{ij} \frac{2}{3} \mu_e \frac{\partial u_k}{\partial u_k}. \quad (4)$$

In the present simulations, the  $k-\varepsilon$  model is employed for turbulence modeling, and the two equations are given as:

Turbulent kinetic energy equation

$$\begin{aligned} & \frac{\partial}{\partial t} (\rho k) + \frac{\partial}{\partial x_j} (\rho u_j k) \\ & = \frac{\partial}{\partial x_j} \left[ \left( \mu + \frac{\mu_t}{\sigma_k} \right) \frac{\partial k}{\partial x_j} \right] + \tau_{ij} \frac{\partial v_i}{\partial x_j} - \rho \varepsilon \end{aligned}. \quad (5)$$

Turbulent kinetic energy dissipation rate equation

$$\begin{aligned} & \frac{\partial}{\partial t}(\rho\varepsilon) + \frac{\partial}{\partial x_j}(\rho u_j \varepsilon) \\ &= \frac{\partial}{\partial x_j} \left( \mu + \frac{\mu_t}{\sigma_\varepsilon} \frac{\partial \varepsilon}{\partial x_j} \right) + \frac{\varepsilon}{k} \left( C_1 \tau_{ij} \frac{\partial v_i}{\partial x_j} - C_2 \rho \varepsilon \right), \end{aligned} \quad (6)$$

where the turbulent viscosity is  $\mu_t$ , and the effective viscosity is defined as

$$\mu_t = \rho C_\mu \frac{k^2}{\varepsilon} \quad \text{and} \quad \mu_e = \mu + \mu_t. \quad (7)$$

## 2.2 Governing equations for droplet phase

According to the two-fluid model, the governing equations for the droplet phase are expressed in Eulerian frame of reference, with respect to the gas phase

Droplet phase continuity equation

$$\frac{\partial \rho_p}{\partial t} + \frac{\partial}{\partial x_j}(\rho_p v_{pj}) = \frac{\partial}{\partial x_j} \left( \frac{v_p}{\sigma_p} \frac{\partial \rho_p}{\partial x_j} \right), \quad (8)$$

Droplet phase momentum equation

$$\begin{aligned} & \frac{\partial \rho_p v_{pi}}{\partial t} + \frac{\partial}{\partial x_j}(\rho_p v_{pj} v_{pi}) = \frac{\partial \tau_{ij,p}}{\partial x_j} \\ & + \frac{\partial}{\partial x_j} \left[ \frac{v_p}{\sigma_p} \left( v_{pi} \frac{\partial \rho_p}{\partial x_j} + v_{pj} \frac{\partial \rho_p}{\partial x_i} \right) \right], \quad (9) \\ & + \frac{\rho_p}{\tau_{rp}} (v_i - v_{pi}) \end{aligned}$$

Droplet phase energy equation

$$\begin{aligned} & \frac{\partial}{\partial t}(\rho_p C_p^p T_p) + \frac{\partial}{\partial x_j}(\rho_p v_{pj} C_p^p T_p) \\ &= \frac{\partial}{\partial x_j} \left( \rho_p C_p^p \frac{v_p}{\sigma_T} \frac{\partial T_p}{\partial x_j} \right) \\ & + \frac{\partial}{\partial x_j} \left( C_p^p v_{pj} C_{n3} \tau_{rp}^2 k_p \frac{\partial \rho_p}{\partial x_j} \frac{\partial T_p}{\partial x_j} \right), \quad (10) \\ & + \frac{\partial}{\partial x_j} \left( C_p^p T_p \frac{v_p}{\sigma_p} \frac{\partial \rho_p}{\partial x_j} \right) + n_p Q_p \end{aligned}$$

Droplet phase turbulent kinetic energy equation

$$\begin{aligned} & \frac{\partial}{\partial t}(\rho_p k_p) + \frac{\partial}{\partial x_j}(\rho_p v_{pj} k_p) \\ &= \frac{\partial}{\partial x_j} \left( \frac{\mu_p}{\sigma_p} \frac{\partial k_p}{\partial x_j} \right) + G_{pk} + G_{gk} \end{aligned}, \quad (11)$$

where the droplet phase stress  $\tau_{ij,p}$  is defined as:

$$\tau_{ij,p} = \mu_p \left( \frac{\partial v_{pi}}{\partial x_j} + \frac{\partial v_{pj}}{\partial x_i} \right) - \delta_{ij} \frac{2}{3} \mu_p \frac{\partial v_{pk}}{\partial x_k}, \quad (12)$$

and the production term of the droplet phase kinetic energy is given by

$$G_{pk} = \mu_p \left( \frac{\partial v_{pi}}{\partial x_j} + \frac{\partial v_{pj}}{\partial x_i} \right) \frac{\partial v_{pi}}{\partial x_j}. \quad (13)$$

As described by Zhou [15], the last source term on the right side of Eq. (11) is the source term due to interaction between the gas phase and the droplet phase through momentum transfer process, which is modeled as:

$$\begin{aligned} G_{gk} &= \frac{2\rho_p}{\tau_{rk}} (C_p^p \sqrt{kk_p} - k_p) \\ & - \frac{1}{\tau_{rp}} \frac{v_p}{\sigma_p} (v_i - v_{pi}) \frac{\partial \rho_p}{\partial x_i}. \end{aligned} \quad (14)$$

The droplet phase turbulent viscosity

$$\mu_p = \rho_p \nu_p \quad \text{and} \quad \nu_p = C_{\mu p} k_p^{0.5} k^{1.5} / \varepsilon. \quad (15)$$

## 2.3 Interaction modeling between the two phases

In this study, two-way coupling between the gas phase and droplet phase, including the momentum and heat transfer. The viscous drag force is expressed in terms of the mechanical droplet response time  $\tau_{rp}$ , which is also called droplet motion relaxation time, given as:

$$\tau_{rp} = \frac{d_p^2 \rho_{pm}}{18\mu} \frac{1}{C_D} \frac{24}{Re_p}, \quad (16)$$

where  $C_D$  is the drag coefficient,  $d_p$  is the droplet diameter,  $\rho_{pm}$  is the material density of the droplets, and  $Re_p$  is the droplet Reynolds number based on the slip velocity between the droplets and the ambient gas flow,

$$Re_p = \frac{\rho |\vec{v} - \vec{v}_p| d_p}{\mu}, \quad (17)$$

The drag coefficient consists of three separate correlations based on the range of  $Re_k$ ,

$$C_D = \begin{cases} 24 / Re_p & Re_p < 1 \\ 24 / Re_p (1 + \frac{1}{6} Re_p^{2/3}) & 1 \leq Re_p \leq 1000 \\ 0.44 & Re_p > 1000 \end{cases} \quad (18)$$

In Eq. (3),  $Q_p$  represents the heat exchange between the gas phase and a single droplet,

$$Q_p = \pi d_p Nu_p \lambda_p (T - T_p). \quad (19)$$

The Nusselt number is defined as:

$$Nu_p = 2.0 + 0.6 Re_p^{0.5} Pr^{0.33}, \quad (20)$$

where  $Pr$  is the Prandtl number  $Pr = \mu C_p^g / \lambda$ , and the  $C_p^g$  and  $\lambda$  are the specific heat capacity and the thermal conductivity of the surrounding gas phase, respectively.

### 3 Numerical methods

The governing equations of the gas and droplet phase are solved by finite differential method. The inviscid flux for the gas phase is computed using Roe scheme, and for the droplet phase, because of the non-hyperbolic nature of the governing equation system, the Flux Vector Splitting (FVS) method is applied to solve the inviscid flux. The face-states are reconstructed by Monotone Upstream-centred Schemes for Conservation Law (MUSCL) method. To avoid un-realistic solutions, a simple modified Harten formulation is applied to satisfy the entropy condition for the Roe scheme [16]. For the viscous flux, second-order accurate central difference scheme is used. A two-step Runge-Kutta method is used to integrate the equations temporally.

## 4 Results and discussions

### 4.1 system description

The test domain is based on the experimental facility in the Virginia Tech supersonic blowdown wind tunnel [17]. The experiments were conducted under the inflow Mach number 3.0 configuration. The geometry of the test section  $200 \times 180$  mm is shown in Fig. 2. The supersonic air flow entered into the domain in the direction parallel to the flat plate from the

left side, and the transverse liquid jet was injected from the wall. The injector orifice was located 80 mm downstream of the leading edge, with a diameter 2.0 mm. Computations made here are run on a  $251 \times 121$  Cartesian grid, as shown in Fig. 3. Due to the strong interaction of the two phases around the injection orifice, a time step  $\Delta t$  was chosen to be  $2.e-9$ s in the current simulation.

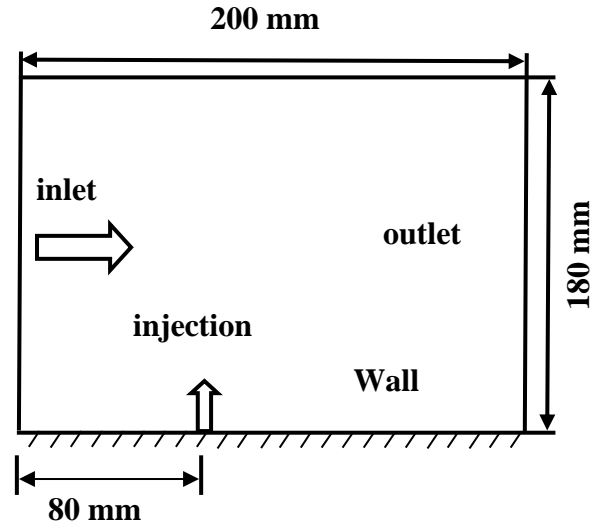


**Fig. 2 Schematic of the injection into the supersonic crossflow.**

The inflow stagnation pressure in the experiment maintained at  $4.5 \text{ atm} \pm 2\%$  and the stagnation temperature was close to the ambient air about  $25^\circ\text{C}$ . The primary parameter used in injection investigations is the jet-to-air momentum flux ratio  $q = \rho_j v_j^2 / \rho_\infty v_\infty^2$ , where  $\rho_j$  and  $\rho_\infty$  are the density of the injected water and the inflow air. In the present study, the computation was conducted under the experimental condition  $q=6$ , and the corresponding mass flow rate of the injected water was maintained at  $90\text{g/s} \pm 1.1\%$  in the experiment. The inlet boundary condition was treated as a supersonic inflow condition, and the outlet variables were obtained through extrapolation. The upside boundary was considered as transparent, and the wall was supposed to be a no-slip boundary.

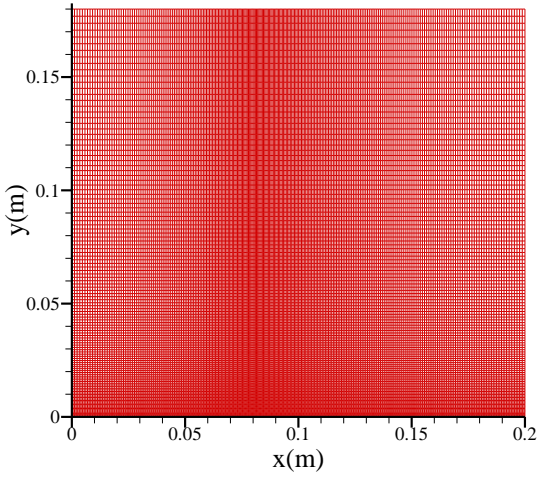


**Fig. 3 Computational grid.**

### 4.2 Penetration height

In the present study, the time evolution of the cross injection into the supersonic flow is obtained. It is interesting to note that the boundary layer detachment, together with the bow shock and the separation shock are well described using the two-fluid model. Fig. 4 shows the consecutive contours of the Mach number. When the injectant penetrates into the supersonic flow, strong drag force due to the high velocity slip between the two phases is acted on the high-speed air, and adverse pressure gradient is formed in front of the injection column, which results in the boundary layer separation and gives rise to the separation shock. The formation of a bow shock attributes to the injection reducing the inflow cross section, and compresses the supersonic flow. Note that, initially, the separation region is small, and the separation shock and bow shock are weak. As the water injected into the main flow, the interaction of the two phases becomes stronger, and alterations in pressure distribution near the injection is induced. The separation point is gradually moving upstream, and makes the separation shock inclined, creating a further change in bow shock angle and jet flow. The continuous vibration of the shock system is called whipping phenomena.

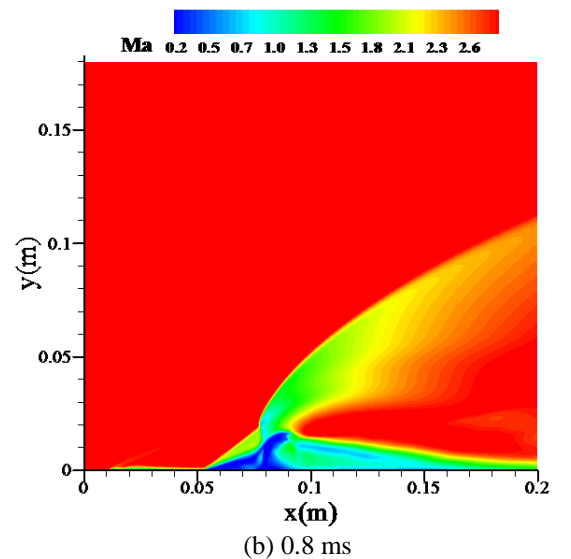
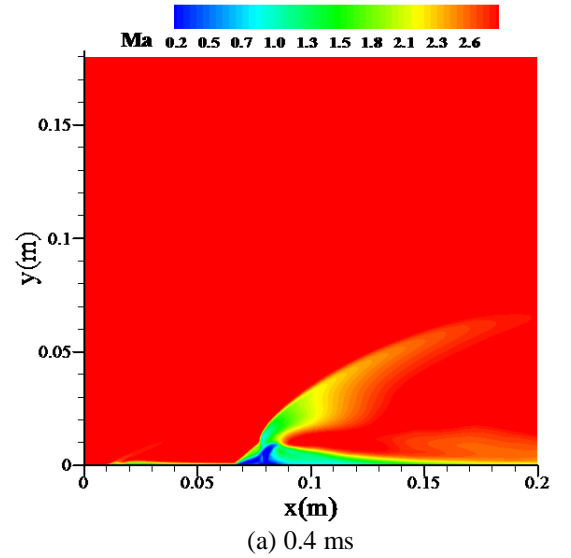
The penetration height was obtained based on the density of the droplet phase. Fig. 5 shows the time evolution of the injection into the supersonic flow. It can be seen that, the injected

liquid column maintains its direction at first. However, as the penetration evolves, the jet is deflected due to the drag force and turns to the inflow direction. Several empirical correlations have been formulated to predict the penetration height of the liquid jets into supersonic crossflow. The expressions for the jet trajectories are commonly described as functions of the momentum flux ratio, the spatial distance from the orifice, and the orifice diameter. The empirical correlations obtained by the shadowgraph and PDPA imaging techniques are, respectively. [7,17]

$$h/d_0 = 3.75(q)^{0.414} (x/d_0)^{0.239}, \quad (22)$$

$$h/d_0 = 4.73(q)^{0.3} (x/d_0)^{0.3}, \quad (23)$$

$$h/d_0 = 3.94(q)^{0.47} (x/d_0)^{0.21}. \quad (24)$$



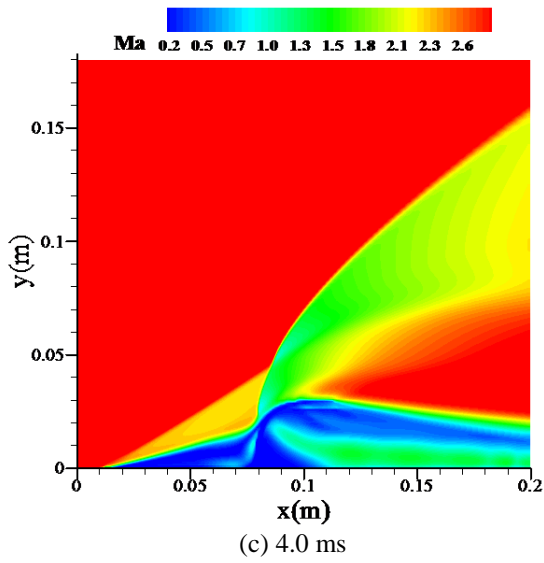


Fig. 4 Time evolutions of the Mach number contours.

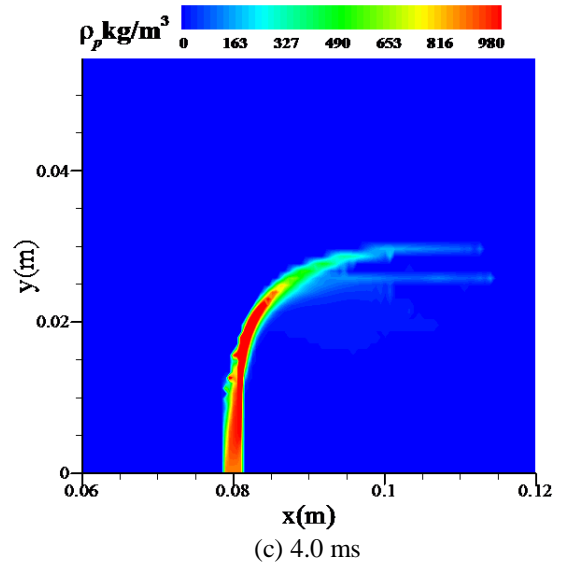
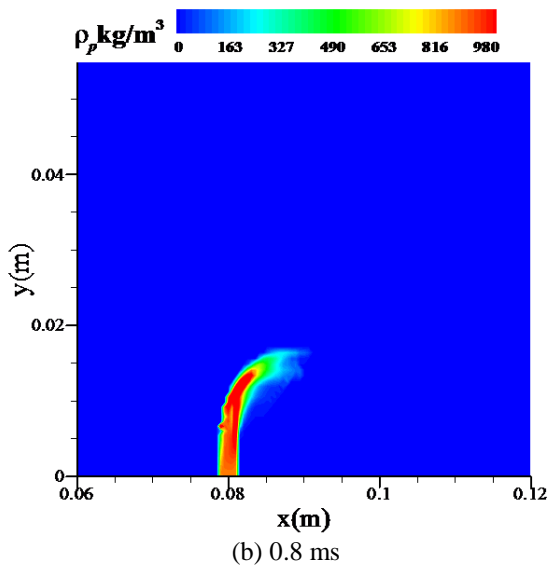
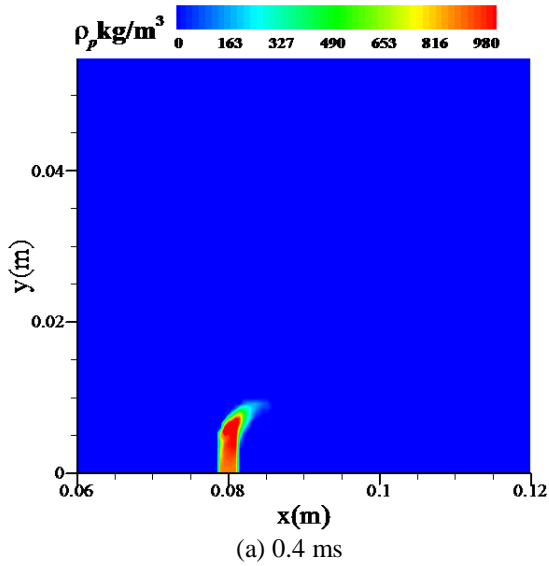


Fig. 5 Time evolutions of the droplet phase density of the jet.



The comparison of the numerical results with the experimental empirical correlations for the jet trajectories is shown in Fig. 6. The penetration height obtained from the simulation is acquired by the centerline of the droplet phase density. It is observed that the predicted trajectory is well matched with the empirical correlations. After about  $8d_0$  from the orifice, the jet starts to incline, and the trajectories turn in the inflow direction, while the increasing of penetration into the main flow slows down. However, in the present study, the breakup of the jet is not considered, so discrepancies exist in the downstream of the trajectories, where the experiments detected the height of the jet increasing more positive than the numerical results, attributing to the smaller droplets stripped from the detaching liquid clumps.

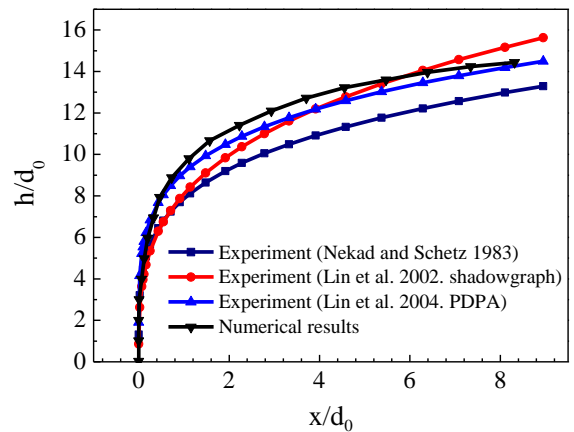


Fig. 6 Trajectories of the numerical results with the predictions from the experimental correlations.

### 4.3 Boundary layer separation

In the process of the liquid jet penetrating into the supersonic flow, separation of the boundary layer can be seen in front of the jet column. The vector contour of the gas phase velocity is shown in Fig. 7. Due to the separation, a circulation zone is formed, and the cross section of the tunnel is reduced for the supersonic inflow. Thus, the resulting separation shock wave is induced. Moreover, the gas phase behind the jet has transferred the momentum to the liquid, and the velocity of the gas phase is decreasing. A low speed area presents in the backside of the injection.

In the boundary layer separation region, the flow velocity decreases to subsonic state which is important to the mixing of the fuel with the air upstream of the injection, and also contributes to the stability of the combustion. The pressure contour is shown in Fig. 8 to illustrate the formation of the adverse pressure gradient leading to the separation of the boundary layer. Note that, the liquid jet give rise to the resistance to the inflow air, and the strong interaction between the gas phase and the liquid jet increases the pressure in front of the jet column. Due to the pressure driven in the boundary layer, the air flows upstream and results in the circulation zone as shown in Fig. 7, and further causes the boundary layer separation. In addition, Fig. 8 gives the interaction point of the separation shock with the bow shock, where high pressure exists and contributes to the inclination of the jet column.

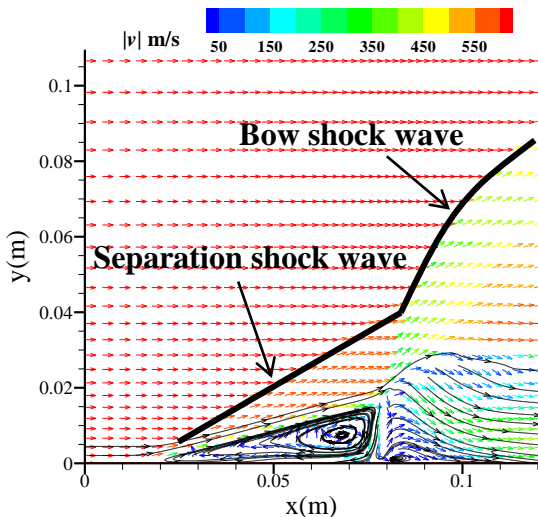


Fig. 7 Vector contours of the gas phase velocity.

Fig. 9 shows the pressure profiles in different  $y$  locations along the direction of the supersonic inflow. It can be seen that the highest pressure in the injection process appears in the shock interaction point. The adverse pressure gradient in the circulation zone is also clearly exhibited on the wall at  $y=0$  mm.

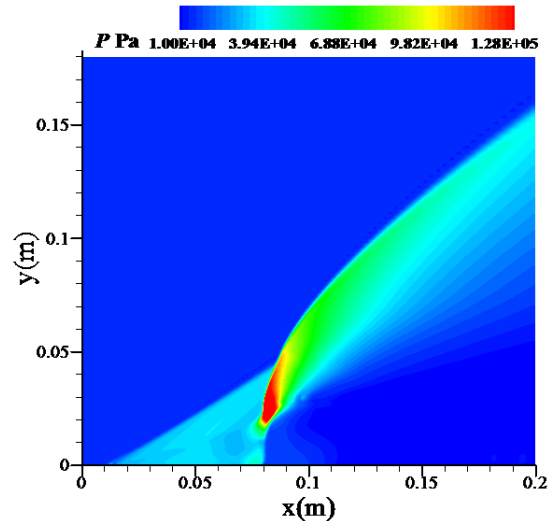


Fig. 8 Pressure contours of the gas phase.

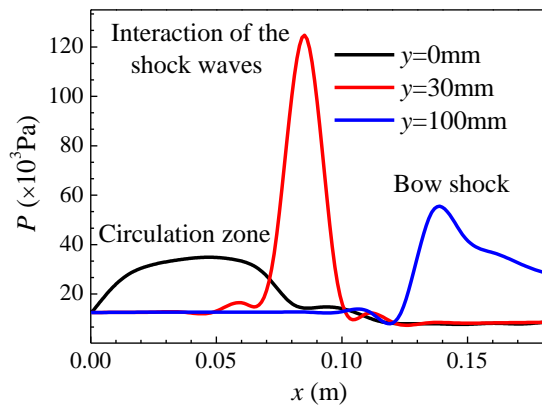
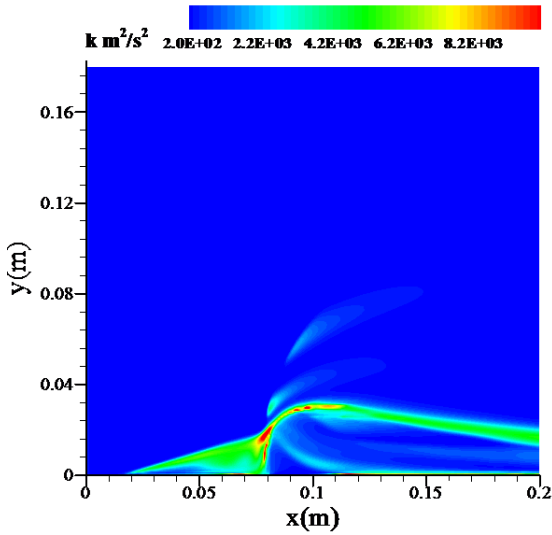


Fig. 9 Pressure profiles along the inflow direction in different vertical locations.

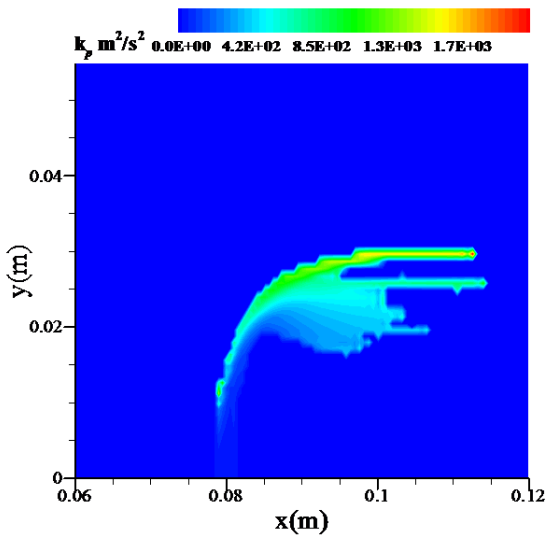
### 4.4 Turbulent kinetic energy for two phases

Fig. 10 shows the turbulent kinetic energy for the air flow and liquid jet. The intensity of the gas turbulence seems to be strong in the circulation zone in front of the jet column, and also in the dividing layer between the liquid and the air. This phenomenon can be explained by the large velocity gradient of the gas phase, which appears in these regions, resulting in strong turbulence there. However, for the droplet phase, the initial part of the jet from the

orifice is not disturbed by the gas phase evidently. As the jet penetrates, in the region where the jet starts to incline to the supersonic inflow direction, the turbulent kinetic energy is increasing. It is consistent with the experiment where the instability of the liquid jet is observed and breakup of the jet column is supposed to be in this region.



(a) Gas phase



(b) Droplet phase

Fig. 10 Turbulent kinetic energy of the gas phase and droplet phase.

#### 4.5 Effects of the momentum flux ratio on the penetration height

The jet-to-air momentum flux ratio is an important parameter that influences the liquid jet penetration height. The empirical correlations also reveal its significance in the experiments. In Fig.11, the predicted trajectories of different momentum flux ratios are compared.

It is shown that the penetration heights are increasing with the momentum flux ratio. The initial part of the injection out of the orifice is similarly perpendicular. However, the inclination points of the jets vary, while the jets with larger momentum flux ratios seem to penetrate more deeply. After the inclination, all of the jet trajectories are almost parallel to each other, and propagate downstream.

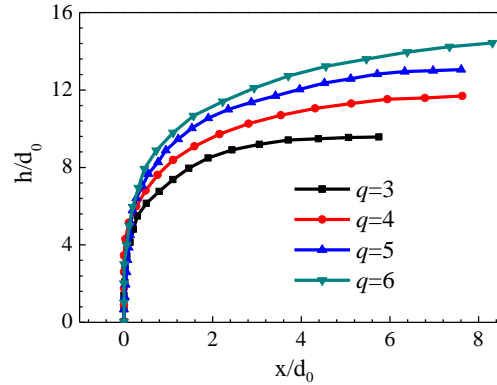
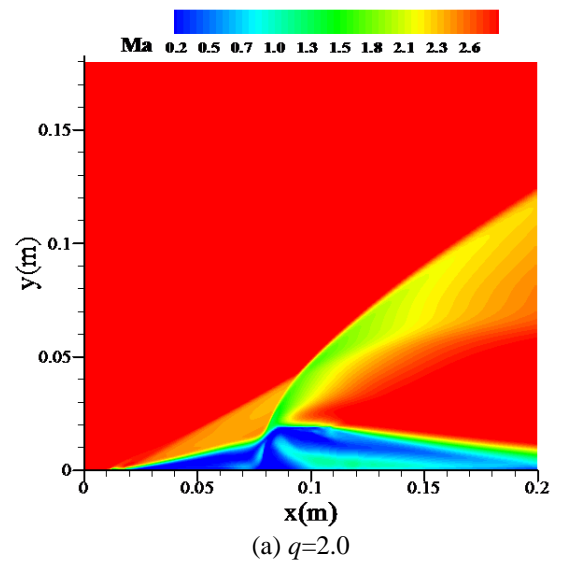


Fig. 11 Droplet trajectories of different jet-to-air momentum flux ratios.

Fig. 12 shows the contours of the Mach number resulted from the momentum flux ratio  $q=2.0$  and  $q=4.0$ . It is noted the momentum flux ratio also affects the gas phase flow field, in particular the angles of the shock waves. As the penetration height increasing with  $q$ , the strength of the bow shock is intensified, and the boundary layer separation becomes larger as the separation point moves upstream, which causes a stronger separation shock.



(a)  $q=2.0$

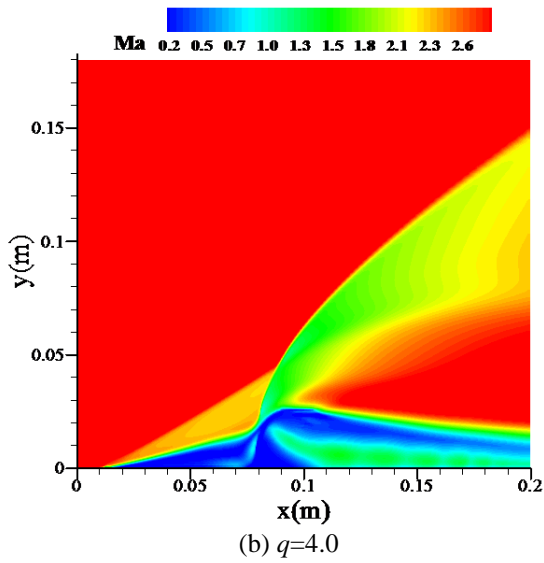


Fig. 12 Mach number contours of different momentum flux ratios.

#### 4.6 Effects of the droplet diameter on the penetration height

There are different sizes of droplets in the liquid injection because of the atomization and breakup. In this section, different diameters of droplets are tested to examine the relationship between the penetration heights with the droplet sizes. In Fig. 13, the trajectories of the jet of droplets varying from 10  $\mu\text{m}$  to 40  $\mu\text{m}$  are obtained from the simulation. It is shown that the larger droplets seem to penetrate higher than the smaller ones. It indicates that the atomization of the jet initially out of the orifice is unfavorable to the jet penetration, though it is considered to contribute to the mixing of the liquid with the crossflow.

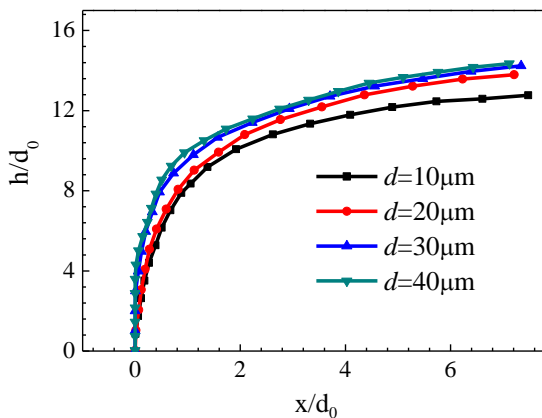


Fig. 13 The trajectories of different droplets.

Fig. 14 shows the contours of the Mach number resulted from the droplets of  $d=10\ \mu\text{m}$  and  $d=40\ \mu\text{m}$ . The difference of the angles of the shock waves caused by the different penetration heights is shown visibly in the contours. In addition, the smaller droplets are supposed to follow the gas closely to get to the backside of the liquid jet, and appear to lead to a lower gas phase velocity zone behind the jet.

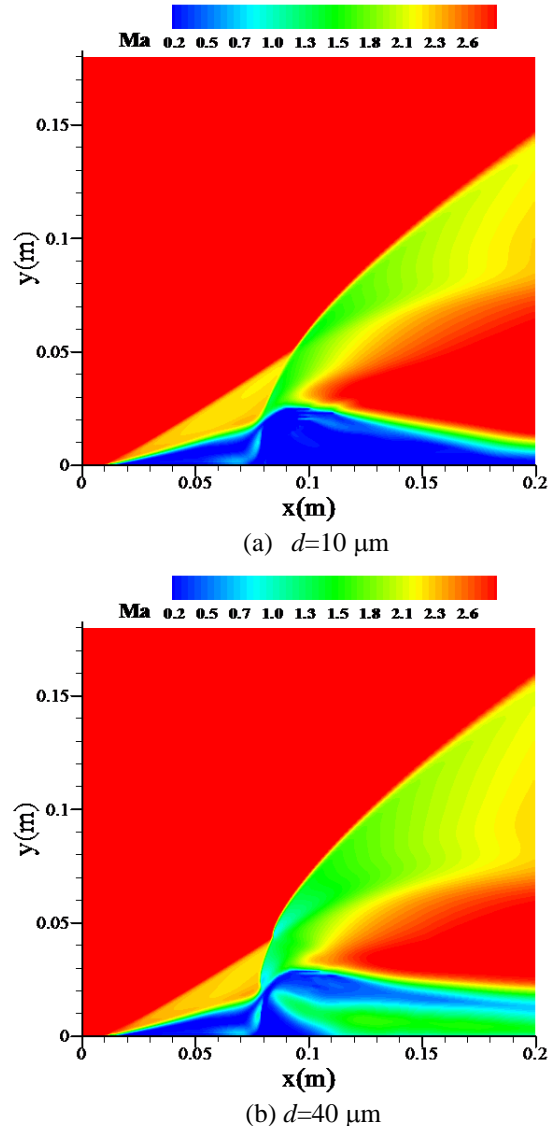


Fig. 14 Mach number contours of different droplets.

## 5 Conclusion

Numerical investigations of the liquid jet into supersonic crossflow have been conducted using the two-fluid method. The boundary layer separation induced by the adverse pressure gradient in front of the injection is captured, and the bow shock wave and the separation shock

wave are obtained as a result. The penetration height predicted by the numerical work has been compared with the empirical correlations derived from experiments, and good agreements are obtained. The present simulation demonstrates that the  $k-\varepsilon-k_p$  turbulence model is adaptable in two-phase compressible flow and gives a reasonable description of the flow field of liquid jet injection into supersonic crossflow. The effects of the jet-to-air momentum flux ratio and the droplet diameter on the penetration height are also investigated in the present work, and larger momentum flux ratio and droplet diameter seem to contribute to the jet penetrate height in the supersonic crossflow.

### Acknowledgment

This work was supported by the National Natural Science Foundation of China under Grant No. 51176099.

### References

- [1] Rachner M, Becker J, Hassa C, and Doerr T. Modelling of the atomization of a plain liquid fuel jet in crossflow at gas turbine conditions. *Aerosp. Sci. Technol.*, Vol. 6, No. 7, pp 495-506, 2002.
- [2] Mathur T, Gruber M, Jackson K, Donbar J, Donaldson W, Jackson T, et al. Supersonic combustion experiments with a cavity-based fuel injector. *J. Propul. Power*, Vol. 17, No. 6, pp 1305-12, 2001.
- [3] Vinogradov VA, Kobigskij SA and Petrov MD. Experimental investigation of kerosene fuel combustion in supersonic flow. *J Propul Power*, Vol. 11, No. 1, pp 130-4, 1995.
- [4] Li J, Ma F, and Yang V. A comprehensive study of combustion oscillations in a hydrocarbon-fueled scramjet engine. *45th AIAA Aerospace Sciences Meeting and Exhibit*, Reno, Nevada, 2007-836, pp 1-12.
- [5] Edward AK, Joseph AS. Liquid jet injection into a supersonic flow. *AIAA J.*, Vol. 11, No. 9, pp 1223-1224. 1973.
- [6] Schetz JA, Kush EA and Joshi PB. Wave phenomena in liquid jet breakup in a supersonic crossflow. *AIAA J.*, Vol. 18, No. 7, pp 774-778, 1980.
- [7] Perurena JB, Asma CO, Theunissen R, and Chazot O. Experimental investigation of liquid jet injection into Mach 6 hypersonic crossflow. *Exp. Fluids.*, Vol. 46, No. 3, pp 403-417, 2009.
- [8] Kyoung SI, Lin KC, and Lai MC. Spray atomization of liquid jet in supersonic crossflows. *43th AIAA Aerospace Sciences Meeting and Exhibit*, Reno, Nevada, 2005-732, pp 1-9.
- [9] Lin KC, Kennedy PJ, and Jackson TA. Spray structures of aerated-liquid jets in subsonic crossflows. *39th AIAA Aerospace Sciences Meeting and Exhibit*, Reno, Nevada, 2001-0330, pp 1-18.
- [10] Lin KC, Kennedy PJ, and Jackson TA. Structure of aerated-liquid jets in high-speed crossflows. *32th AIAA Fluid Dynamics Conference and Exhibit*, St. Louis, Missouri, 2002-3178, pp 1-12.
- [11] Sallam KA, Aalburg C, Faeth GM, Lin KC, Carter CD and Jackson TA. Breakup of aerated-liquid jets in supersonic crossflows. *42th AIAA Aerospace Sciences Meeting and Exhibit*, Reno, Nevada, 2004-970, pp 1-10.
- [12] Lin KC, Kennedy PJ, and Jackson TA. Structure of water jets in a Mach 1.94 supersonic crossflow. *42th Aerospace Sciences Meeting and Exhibit*, Reno, Nevada, 2004-971, pp 1-19.
- [13] Zheng Y, Wan, XT, Qian Z, Wei F and Jin Y. Numerical simulation of the gas-particle turbulent flow in riser reactor based on  $k-\varepsilon-k_p-\varepsilon_p-\Theta$  two-fluid model. *Chem. Eng. Sci.*, vol. 56, pp 6813-6822, 2001.
- [14] Enwald H, Peirano E and Almstedt AE. Eulerian two-phase flow theory applied to fluidization. *Int. J. Multiph. Flow*, Vol. 22, pp 21-66, 1996.
- [15] Zhou LX. *Theory and numerical modeling of turbulent gas-particle flows and combustion*. Science Press and CRC Press, 1993.
- [16] Kermani MJ and Plett EG. Modified entropy correction formula for the Roe scheme. *AIAA, Inc* 2001.
- [17] Thomas RH and Schetz JA. Distributions across the plume of transverse liquid and slurry jet in supersonic airflow. *AIAAJ.*, Vol 23, No. 12, pp 1892-1901, 1985.

### Contact Author Email Address

E-mail to: [guoyc@tsinghua.edu.cn](mailto:guoyc@tsinghua.edu.cn)

### Copyright Statement

The authors confirm that they, and/or their company or organization, hold copyright on all of the original material included in this paper. The authors also confirm that they have obtained permission, from the copyright holder of any third party material included in this paper, to publish it as part of their paper. The authors confirm that they give permission, or have obtained permission from the copyright holder of this paper, for the publication and distribution of this paper as part of the ICAS 2014 proceedings or as individual off-prints from the proceedings.